REMOTE SENSING OF ENVIRONMENT 18:000–000 (1987)

A Model for Soil Surface Roughness Influence on the Spectral Response of Bare Soils in the Visible and Near-Infrared Range

JERZY CIERNIEWSKI

Agricultural University in Poznan, Department of Ameliorative Pedology, ul. Wojska Polskiego 71 E, 60-625 Poznan, Poland

A mathematical model dealing with the influence of soil surface roughness on soil reflectance in the visible and near-infrared range is discussed. The model is based on the assumption that the reflectance from anisotropic rough soil surfaces is strongly correlated with the area of shadowed soil fragments, and therefore depends on the degree of soil roughness as well as on the illumination and the viewing geometry. A rough soil surface is simulated by equal-sized spheres arranged such that their centers form a square grid on a freely sloping plane. This model converts the bare soil reflectance data obtained for smooth samples into data relating to any natural rough surface states under conditions of unlimited illumination, which are defined by the solar altitude, the angle of a slope, and the sloping of the soil surface relating to the sunbeams direction. A simple parameter of the state of soil roughness expressing a proportion of the aggregates' and clods' area in top view in a given soil surface area is used here. The correctness of this model was evaluated on spectral data from 12 air-dried undisturbed soil samples obtained by means of a field spectrophotometer in outdoor conditions at solar altitudes from 31° to 59°. The measurements were taken for soil surfaces sloping at angles of 0°, 10°, 20°, and 30° forward and backward to the direction of sunbeams. Linear regression analysis indicates that for the studied spectral range the correlation coefficient of the relationship between all the 368 data point measured and calculated using this model reaches values of approximately 0.99. It has been found that relation between measured and predicted reflectance coefficient is similar for all the tested soils.

Introduction

The roughness of soil surface is one of the most important factors influencing the reflectance characteristics of bare soils in the visible and near-infrared range. Yet the conclusion about the influence of roughness on soil reflectance, as determined by laboratory studies on disturbed samples (Belonogova and Tolchelnikov, 1959; Bowers and Hanks, 1965; Gerbermann and Weher, 1979; Kondratyev and Fedchenko, 1980; Mikhaylova and Orlov, 1985; Obukhov and Orlov, 1964; Piech and Walker, 1974) may not be compared directly with the same relationships defined under field conditions. This is due not only to the more complicated roughness of natural soil surfaces, but also to the dissimilarity of soils illumination conditions. Because of these outside conditions during soil spectral measurements, one can assume that anisotropic rough soil surfaces are not perfect diffusing matter, and thus their spectral characteristics also depend on sun–soil surface–sensor geometries (Egbert and Ulaby, 1972; Guyot, 1984; Epiphanio and Vitorello, 1984; King, 1984).

The aim of this paper is presentation and evaluation of the accuracy of a mathematical model which converts the spectral data for reflectance of bare soils obtained on smooth samples into data valid for any soil roughness state under unlimited illumination conditions, as de-

52 Vanderbilt Ave., New York, NY 10017

0034-4257/87/$3.30

termined by the solar altitude, the angle of slopes, and the sloping towards the sunbeams direction.

Methods

The model

The model assumes that the amount of reflected direct beam energy in the visible and near-infrared range from anisotropic soil surfaces is strongly correlated with the shadowed area per unit area of soil fragments. This proportion, called the shadowing coefficient of soil surface (SC_n), besides the degree of soil surface roughness, also depends on the direction of illumination, direction of view, and the slope aspect of the soil surface. In the first stage, the model calculates as a function of these variables the SC value in relation to a nadir-looking sensor. A natural rough soil surface is simulated by equal sized spheres arranged so their centers form a square grid on a freely sloping plane (Fig. 1). The roughness factor of this structure (RF_m) is defined as:

$$RF_m = A_s/A_u, \qquad A_s = \pi\phi^2/4,$$
$$A_u = d^2\cos\gamma, \tag{1}$$

where A_s = area of a sphere from top view, A_u = unit of area, ϕ = diameter of the spheres, d = distance between spheres, and γ = angle of slope. The relationship between d and RF_m is then given by the formula:

$$d = \frac{\phi}{2}\left(\frac{\pi}{RF_m}\cos\gamma\right)^{1/2}. \tag{2}$$

This structure, forward or backward sloping to the sunbeams direction, is illuminated by the sunbeams lying in planes

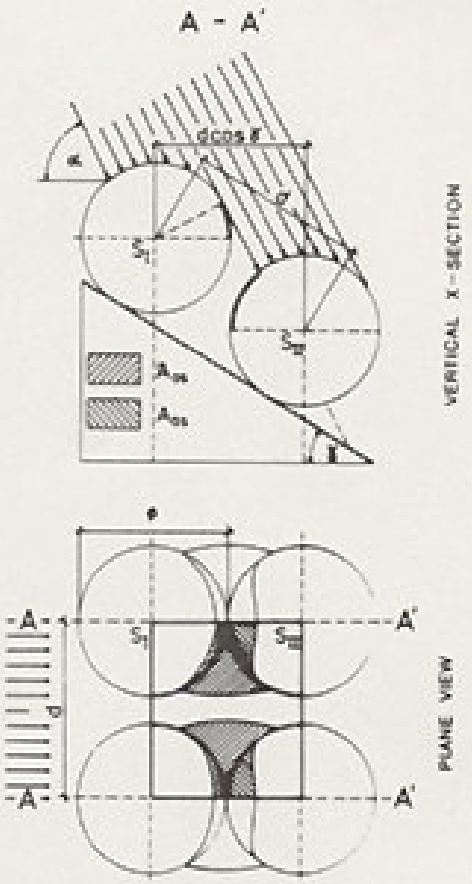

FIGURE 1. Geometry of simulated surface shadow for calculation of the roughness factor (RF_m) and the shadowing coefficient (SC_m).

parallel to the net quarter sides. For the determination of the shadowing coefficient of the modelled surface (SC_m), similarly as for natural rough surfaces (SC_n), we must know the total shadowed area of this structure in a given area unit of the horizontal projection. Sphere S_I cast this total shadowed area which includes two components. One component (A_{os}) includes the shadowed areas both on the sphere S_I and on the planar surface. The other component (A_{ss}) includes an area on the nearby sphere S_{II} that is shaded by sphere S_I. The SC_m may be written as

$$SC_m = \frac{A_{os} + A_{ss}}{A_u}. \tag{3}$$

The values of shadow components were found analytical by solving trigonometric

equations describing the position of the respective shadow elements in a coordinate system having its origin in the center of the sphere S_I or S_{II}.

When the roughness factor of the modelled surface is so low under the given illumination conditions that the adjoining sphere S_{II} does not overlap its shadow on the planar slope, that is, $d\cos\gamma \geq d_e + a_e + \phi/2$, the first component ($A_{os1}$) is calculated as follows (Fig. 2). The distance of the shadow ellipse center from the given sphere center (d_e) and the major axis of the shadow ellipse (a_e) in top view are defined as follows.

For the forward slope as:

$$d_e = \frac{\phi}{2}\cos\gamma\left[\tan(90-\alpha-\gamma)+\tan\gamma\right], \tag{4a}$$

$$a_e = \frac{\phi}{2}\frac{\cos}{\cos(90-\alpha-\gamma)}. \tag{5a}$$

For the backward slope as:

$$d_e = \frac{\phi}{2}\cos\gamma\left[\frac{1}{\tan(\alpha-\gamma)}-\tan\gamma\right], \tag{4b}$$

$$a_e = \frac{\phi}{2}\frac{\cos\gamma}{\sin(\alpha-\gamma)}, \tag{5b}$$

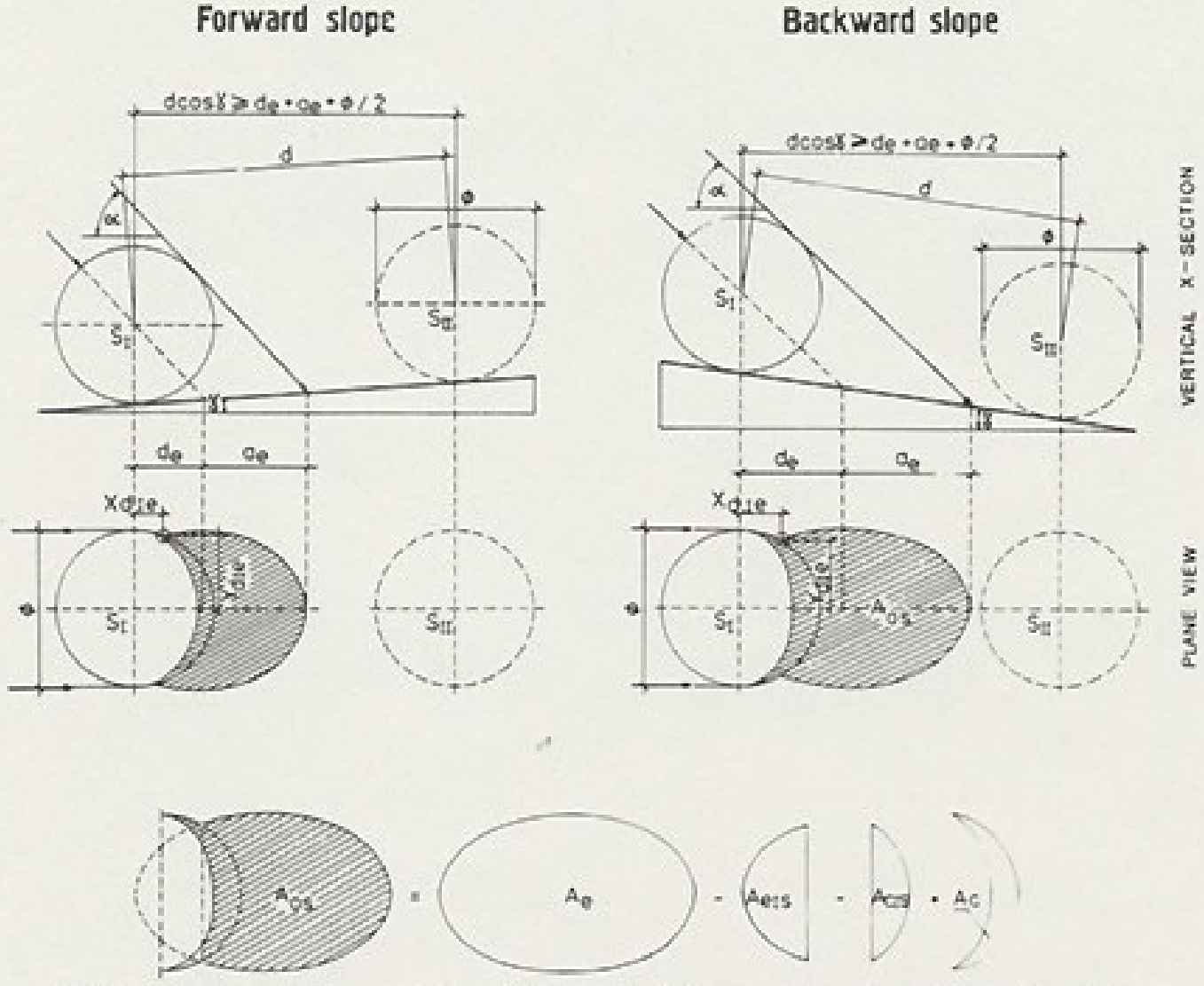

FIGURE 2. Geometry of an own-sphere shadow and a shadow on a slope plane cast by a given sphere.

where α = solar altitude. Solving the system of equations

$$x^2 + y^2 - \frac{\phi^2}{4} = 0,$$

$$\frac{(x - d_e)^2}{a_e^2} + \frac{4y^2}{\phi^2} - 1 = 0,$$

describing a circle of the sphere S_I and the shadowed ellipse by the d_e and a_e, the distance of the intersection point of the sphere and the shadow ellipse from the given sphere center in the horizontal projection (X_{dIe}, Y_{dIe}) is defined as

$$X_{dIe} = \phi \frac{d_e}{(\phi + 2a_e)}, \tag{6}$$

$$Y_{dIe} = \left(\frac{\phi^2}{4} - X_{dIe}^2\right)^{1/2}. \tag{7}$$

We can then calculate the total area of the first shadow component (A_{os1}) as the algebraic sum of the following figure areas:

$$A_{os1} = A_e + A_{eIs} - A_{cIs} + A_c,$$

where

$$A_e = \pi \frac{\phi}{2a_e},$$

$$A_{eIs} = \frac{\phi}{2} a_e \arccos \frac{d_e - X_{dIe}}{a_e} - (d_e - X_{dIe}) Y_{dIe},$$

$$A_{cIs} = \frac{\phi^2}{4} \arccos \frac{2X_{dIe}}{\phi} - X_{dIe} Y_{dIe},$$

$$A_c = \pi \frac{\phi^2}{8} (1 - \sin \alpha). \tag{8}$$

If the surface roughness factor is high enough so that under the given conditions the shadow on the slope plane is overlapped by the adjoining sphere S_{II}, that is, if $d \cos \gamma < d_e + a_e + \phi/2$, this first shadow component (A_{os2}) is correspondingly reduced (Fig. 3). The distance of the intersection point of sphere S_{II} and the shadow ellipse from the assumed origin of the coordinates at the horizontal projection (X_{dIIe}, Y_{dIIe}) was solved from

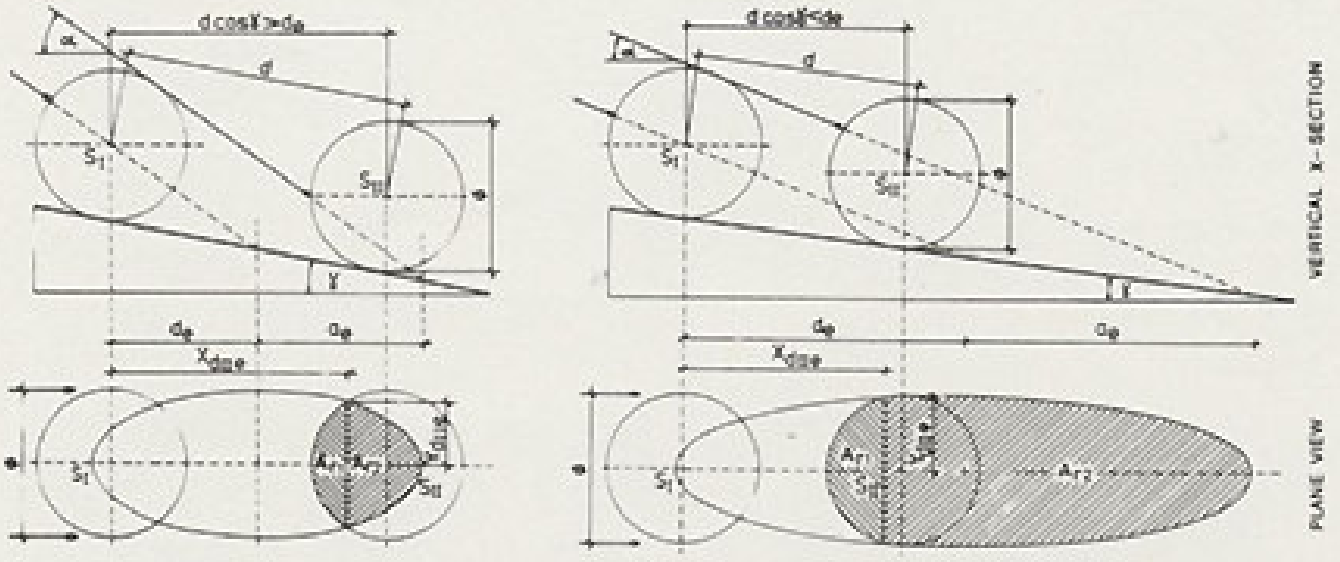

FIGURE 3. Geometry of shadow reduction on a slope plane due to an adjoining sphere.

the system of equations

$$x^2 + y^2 - \frac{\phi^2}{4} = 0,$$

$$\frac{(x \pm d\cos\gamma \pm d_e)^2}{a_e^2} + \frac{4y^2}{\phi^2} - 1 = 0.$$

The position of this point is finally expressed by the formula:

$$X_{d\mathrm{II}e} = \frac{\phi d_e + 2da_e\cos\gamma}{\phi + 2a_e}, \text{ if } d\cos\gamma \geqslant d_e \quad (9a)$$

$$X_{d\mathrm{II}e} = \frac{\phi d_e - 2da_e\cos\gamma}{\phi - 2a_e}, \text{ if } d\cos\gamma < d_e, \quad (9b)$$

$$Y_{d\mathrm{II}e} = \left[\frac{\phi^2}{4} - (d\cos\gamma - X_{d\mathrm{II}e})^2\right]^{1/2}, \quad (10)$$

which make it possible to calculate the first shadow component's reduction as the sum of two values $(A_{r1} + A_{r2})$, the first of which is calculated as

$$A_{r1} = (\phi^2/4)\arccos[(2/\phi) \times (d\cos\gamma - X_{d\mathrm{II}e})] - (d\cos\gamma - X_{d\mathrm{II}e})Y_{d\mathrm{II}e}, \quad (11)$$

while the second (A_{r2}) depends on the position of the point $(X_{d\mathrm{II}e}, Y_{d\mathrm{II}e})$ in relation to the center of adjoining sphere S_{II}, and is calculated as follows:

If $d\cos\gamma \geqslant d_e$ *as*

$$A_{r2} = \frac{\phi}{2}a_e\arccos\frac{d_{\mathrm{II}e} - d_e}{a_e} - (X_{d\mathrm{II}e} - d_e)Y_{d\mathrm{II}e}; \quad (12a)$$

If $d\cos\gamma < d_e$ *as*

$$A_{r2} = \pi\frac{\phi}{2}a_e - \left[\frac{\phi}{2}a_e\arccos\frac{d_e - X_{d\mathrm{II}e}}{a_e} - (d_e - X_{d\mathrm{II}e})Y_{d\mathrm{II}e}\right]. \quad (12b)$$

Thus the total area of the first shadow component (A_{os2}) may be expressed by the formula:

$$A_{os2} = A_{os1} - (A_{r1} + A_{r2}). \quad (13)$$

On sphere S_{II}, the additional shadowed area (A_{as}) cast by sphere S_{I} can be viewed only by a nadir-looking sensor when A_{as} is situated above the S_{II} sphere's "equator," i.e., if the condition that $r_{\min} < \phi/2$ is satisfied (Fig. 4). The $r_{\min}$ formula was found from an equation describing a sunbeam tangential to the sphere S_{I} passing at a distance r from the S_{I} sphere center,

$$y = \pm\tan\alpha\, x + \frac{r}{\cos\alpha} + d(\pm\tan\alpha\cos\gamma \pm \sin\gamma)$$

with assumption that $y = 0$ and $x = r$. This formula for the forward slope is

$$r_{\min} = d\cos\alpha\frac{\tan\alpha\cos\gamma + \sin\gamma}{1 + \sin\alpha}, \quad (14a)$$

and for the backward slope,

$$r_{\min} = d\cos\alpha\frac{\tan\alpha\cos\gamma - \sin\gamma}{1 + \sin\alpha}. \quad (14b)$$

Half of the A_{as} shadow's width $(1_{\max})$ is expressed by the equation

$$1_{\max} = \left(\frac{\phi^2}{4} - r_{\min}^2\right)^{1/2}. \quad (15)$$

The intersection of the sunbeams (which are tangential to the S_{I} sphere and project the outline of the A_{as} shadow on the S_{II} sphere) with the S_{II} sphere was ob-

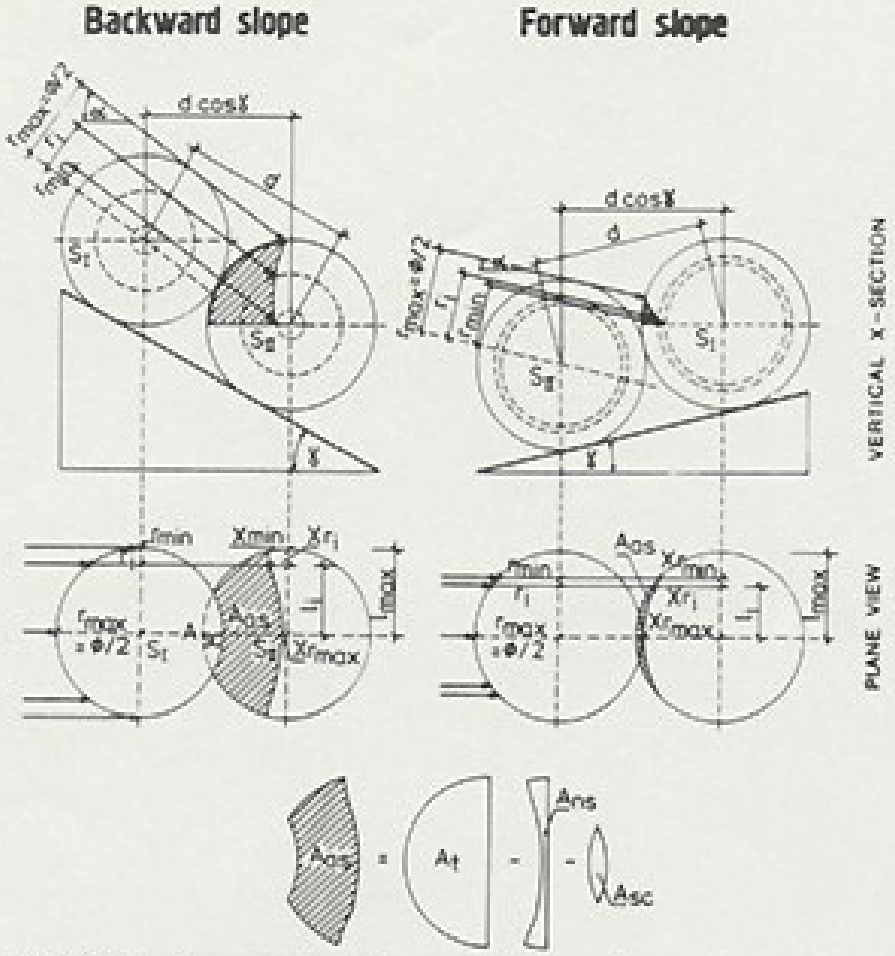

FIGURE 4. Geometry of a shadow on a sphere cast by an adjoining sphere.

tained by solving the equations system

$$y = \pm \tan\alpha\, x + r_i \cos\alpha + d(\pm \tan\alpha \cos\gamma \pm \sin\gamma),$$

$$x^2 + y - r^2 = 0.$$

Position of this point (X_{ri}), as determined by the sunbeams passing at a distance of r_i from the center of sphere S_{II} is defined for the forward slope as

$$X_{ri} = -\cos^2\alpha\left[\frac{r_i \tan\alpha}{\cos\alpha} - dM\tan\alpha - \left(\frac{2r_i dM}{\cos\alpha} - d^2M^2\right)^{1/2}\right],$$

where

$$M = \sin\gamma + \tan\alpha\cos\gamma, \qquad (16a)$$

and for the backward slope as

$$X_{ri} = -\cos^2\alpha\left[\frac{r_i \tan\alpha}{\cos\alpha} + dN\tan\alpha - \left(\frac{-2r_i dN}{\cos\alpha} - d^2N^2\right)^{1/2}\right],$$

where

$$N = \sin\gamma - \tan\alpha\cos\gamma. \qquad (16b)$$

The no shadow area on the S_{II} sphere in top view (A_{ns}) defined as

$$A_{ns} = 2\int_0^{l_{max}} f(X_{ri})\, dl \qquad (17)$$

can be solved by the Simpson's approximation, using Eq. (16a) or (16b) and expressing the r_i parameter by the l_i

variable as

$$r_i = \left(\frac{\phi^2}{4} - l_i^2\right)^{1/2}. \qquad (18)$$

Finally, the shadow area (A_{as}) is given by

$$A_{as} = A_t - A_{ns} - A_{sc},$$

where

$$A_t = \pi\frac{\phi^2}{8} - \frac{\phi^2}{4}\arccos\frac{2l_{max}}{\phi} + l_{max}r_{min},$$

$$A_{sc} = \tfrac{1}{2}\left[\phi^2\arccos\frac{d\cos\gamma}{\phi} - d\cos\gamma\left(\phi^2 - d^2\cos^2\gamma\right)^{1/2}\right] \qquad (19)$$

with the limitation that the A_{sc} element refers only to the backward slope when $\phi > d\cos\gamma$.

In the second step after calculation of the shadowing coefficient of soil surface (SC_m) by the above formulas, we assume that there is an exponential relationship betwen the SC_m and the reduction of the soil reflectance level in relation to data for the same soil but smooth and dry (β_λ):

$$\beta_\lambda = a\exp(bSC_m).$$

The constants a and b (Table 1) are derived from laboratory spectrophotometric studies of soils (Cierniewski, 1986).

TABLE 1 Constants of Eq. (25)

Wavelengths λ (nm)	a	b
40	0.976	−1.462
540	0.980	−1.324
640	0.979	−1.261
740	0.978	−1.074
860	0.977	−1.089

Soil analysis

The accuracy of this model was evaluated using typical soils of the Koscian diluvial plateau in Wielkopolska Lowland situated in western Poland. Twelve air-dried undisturbed soil samples characterizing natural rough surface horizons of these soils after ploughing and 12 samples of the same soils having artificially smooth surfaces were used for this evaluation. These samples were photographed by a 58-mm small format camera to record the samples' (RF_n) roughness state. Once enlarged, the photographs enabled us to separate the natural soil aggregate and clod contours and to measure their area in the top view by means of Cambridge Quantimet 720 image analysis computer made by Imanco.

These samples were classified in the field according to the standard soil profile description. In the laboratory their mechanical composition was determined by the areometric method, and organic matter content by loss-on-ignition when burned at temperature of 460°C.

Spectral measurements

Soil samples were placed in 65×65 cm dishes of 5 cm depth, and viewed by a SPZ-02 field spectrophotometer under outdoor conditions. This spectrophotometer, constructed at the Space Research Centre in Warsaw, is a 24-channel circular-variable filter instrument. It measures the amount of energy at wavelengths from 0.4 to 1.06 μm which enters the instrument as the filters are rotated through the two optical paths. The first of these looks at the measured object,

TABLE 2 Solar Altitudes (α) at Which Soil Spectral Data Were Collected and Number of Measurements Corresponding to Them[a]

Sample	Solar Altitudes for		Number of Measurements for			Total
	Forward	Backward				
No.	Slope (fs)	Slope (bs)	(fs)	(bs)	(hs)	Number
1	40,48,58	36,44,51,56	9	12	7	28
2	40,48,48.5,51,58	35.5,44	15	6	7	28
3	40,47,49,58.5	35,44,51,55	12	12	8	32
4	41,47,57.5,58.5	35,44.5,55	12	9	7	28
5	41.5,46,49,58	34.5,45,55,58	12	12	8	32
6	41.5,46,49,58	34.5,45,55,58	12	12	8	32
7	42,46,49.5,58,58	34,45,55	15	9	8	32
8	42.5,45.5,50,58	33,46,54,58	12	12	8	32
9	43,45.5,50,58	32.5,46,54,58	12	12	8	32
10	42,46,50,58	33.5,45.5,54,58	12	12	8	32
11	43.5,45,50.5,58	31.5,46.5,58	12	9	7	28
12	43,45,50.5,58	32,46,54,58	12	12	8	32
		Total	147	129	92	368

[a]At each solar altitude for both forward and backward slopes, spectral measurements were taken at slope of 0°, 10°, and 30°. For a horizontal position of soil (hs), data were collected at identical solar altitudes, as for forward and backward slopes.

and the second is a comparative path equipped with a diffusing plate situated at the top of the spectrophotometer. The light energy passing through these paths leads to a semiconductor diode sensor. The hemispherical-directional reflectance coefficient for each wavelength is determined by comparing the amount of energy reflected from the analyzed object with the amount of energy incident on the diffusing plate. Barium sulfate standard plate was used for calibration of this instrument. The output signals of the spectrophotometer are recorded on a magnetic tape, allowing data processing by a microcomputer. All spectra were obtained vertically at a distance of 2.14 m from the sample. The 15° field of view of this instrument integrates energy from a horizontally situated area of 0.25 m^2, having a 56.4 cm diameter.

The reflectance data for the natural rough samples (R_r) were collected on 24 July 1985 between 7:18 am and 3:08 pm GMT, and for the smooth samples (R_s) on the next day between 1:54 pm and 2:08 pm GMT. When the sky was clear and the solar altitude varied from 41° to 43°. While the smooth soil samples were always horizontal during measurement, the samples of natural rough soils were at various angles, both horizontal and oblique. The illumination data of the rough samples during measurement is presented in Table 2.

Results

The model

The shadowing coefficient of soil surface (SC_m) is calculated for those slope angles which were examined experimentally, i.e., 0°, 10°, 20°, and 30° (Fig. 5). The SC_m was assumed to reach a value of 1 for the backward slope, because complete shadowing of a soil slope occurs when the solar altitude is lower than the angle of a given slope. Under all remaining situations on the backward and for-

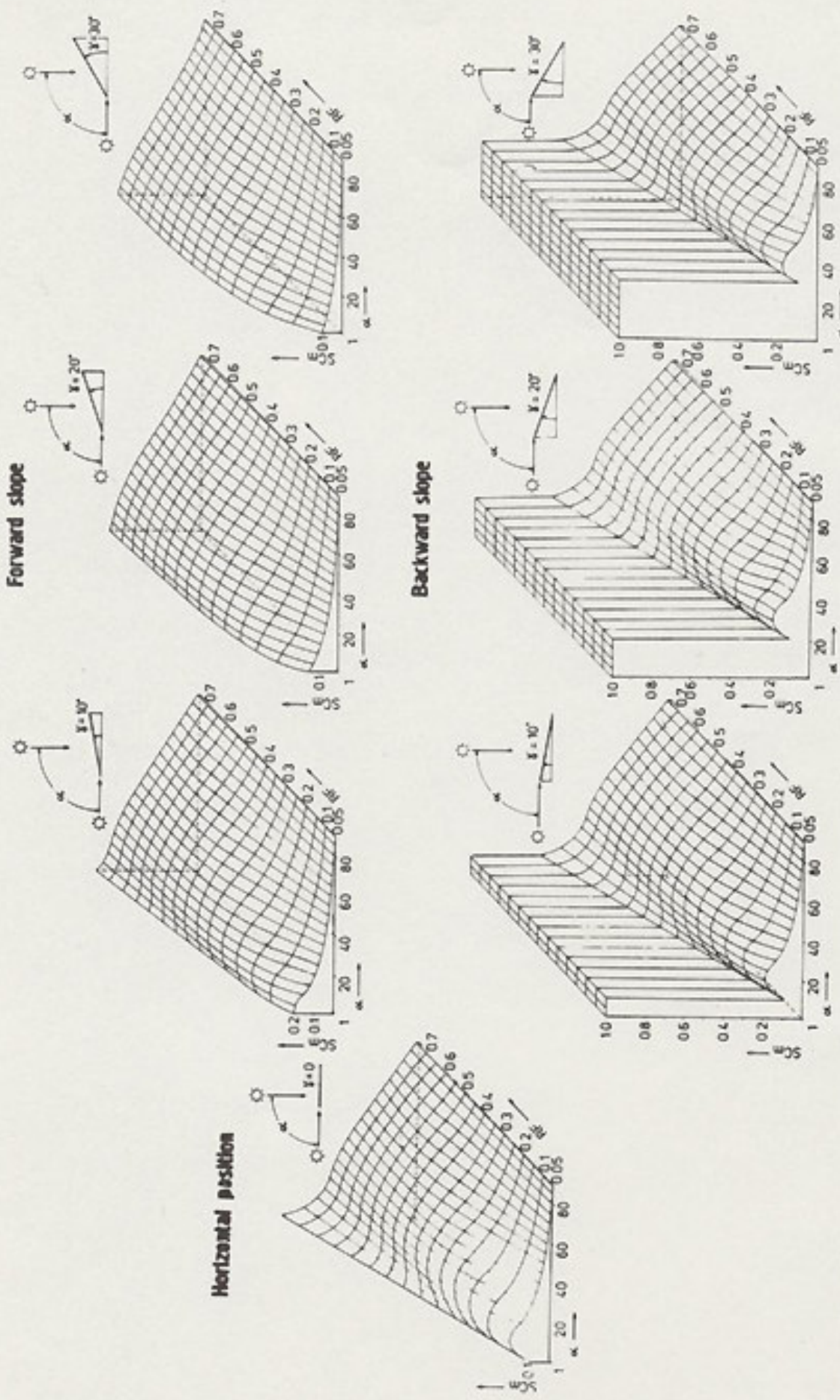

FIGURE 5. Relationship between the simulated shadowing coefficient of soil surface (SC_m) and the rough soil surface factor (RF_m), the solar altitude (α), and the slope angle of soil surface (γ).

ward slopes and also in the horizontal position, soil surface shadowing decreases when soil roughness decreases. The SC_m decreases with an increase of the solar altitude over the full range from 0° to 90° only for the soil on forward slopes more sloping than 20°. An opposite relationship may occur for a specified range of solar altitude when the surface roughness factor (RF_m) is lower than 0.5. This interval, where the soil shadowing increases with the sun's rising, decreases with an increase of the sloping angle. For backward slopes it moves in the direction of higher solar altitudes, nearing the numerical values of the slope angles.

The function used in the second step of this modeling described the relationship between the soil surface shadowing coefficient (SC_m) and the reduction of the soil reflectance level (β_λ). The relation is similar for the five analyzed wavelengths (Fig. 6). The β_λ approaches 1 for an absence of soil surface shadowing (when $SC_m = 0$), while for full shadowing of a soil surface (when $SC_m = 1$) it is between 1/4 and 1/3. As a result, this model predicts that the shapes of the rough soil curves and the smooth soil curves will be similar, but their levels will be different.

Studied soils

In the Polish system of classifying soils, the soils used to evaluate the model belong to initial loose denudative soils, typic brown podsolic soils, eroded (with Bt horizon on the surface) brown podsolic soils, typic black earths, and degraded black earths. The descriptions of these soils, together with their approximate equivalents under the American soil classification system, are listed in Table 3.

Aggregates and clods of the studied soil surface samples are shown in Fig. 7. The initial loose denudative soils formed the

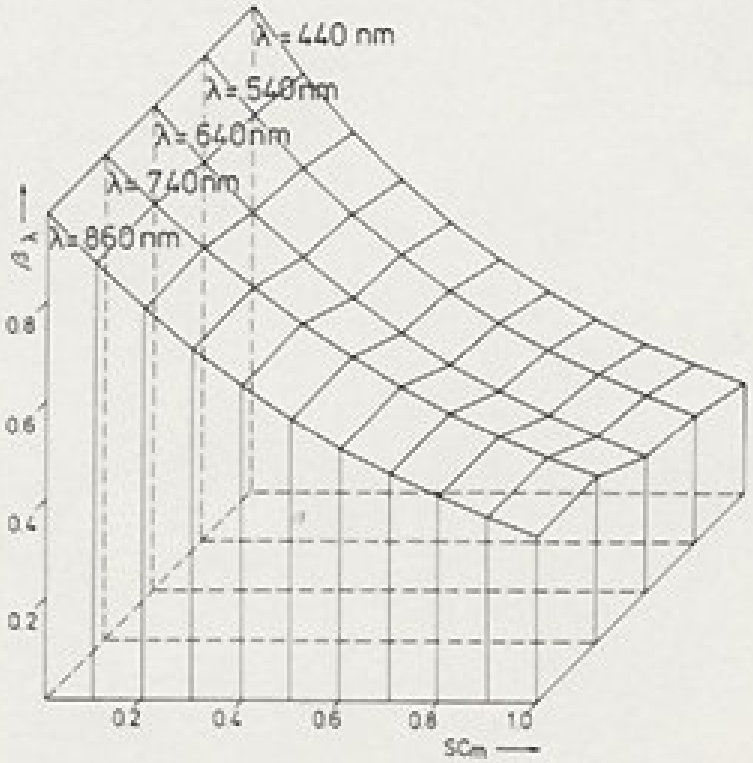

FIGURE 6. Relationship between the shadowing coefficient of soil surface (SC_m) and the reduction of the soil reflectance level (β_λ).

TABLE 3 Description of the Studied Soils[a]

SNo	Ss	Soil	Order	Texture	Content of Sand (%)	Silt (%)	Clay (%)	OM (%)	Dry Munsell Color	RF_n
1	Id	Initial loose denudative soil	Entisol	sand	89	10	1	0.6	10YR7/3	0.08
2	Id	Initial loose denudative soil	Entisol	sand	91	8	1	0.9	10YR6/3	0.06
3	Bt	Typic brown podsolic soil	Alfisol	loamy sand	78	21	1	1.1	10YR7/2	0.35
4	Bt	Typic brown podsolic soil	Alfisol	loamy sand	78	20	2	1.8	10YR6/3	0.27
5	Be	Eroded brown podsolic soil	Alfisol	sandy loam	66	23	11	1.6	10YR6/4	0.51
6	Be	Eroded brown podsolic soil	Alfisol	sandy loam	69	18	13	1.7	10YR6/4	0.51
7	Db	Degraded black earth	Mollisol	loamy sand	74	23	3	2.8	10YR3/2	0.39
8	Dd	Degraded black earth	Mollisol	sandy loam	56	40	4	3.1	10YR3/2	0.46
9	Dd	Degraded black earth	Mollisol	sandy loam	62	31	7	3.6	10YR3/2	0.45
10	Dt	Typic black earth	Mollisol	sandy loam	69	30	1	4.2	10YR3/1	0.50
11	Dt	Typic black earth	Mollisol	sandy loam	59	37	4	4.3	10YR3/1	0.50
12	Dt	Typic black earth	Mollisol	sandy loam	64	31	5	4.7	10YR2/3	0.43

[a]SNo = sample number; Ss = symbol of soil; RF_n = soil surface roughness factor; OM = organic matter content.

least rough surfaces. These surfaces had no clods larger than 20 mm in diameter and had natural rough soil surface factors (RF_n) lower than 0.1. The largest clods of typic brown podsolic soil surfaces do not exceed 50 mm diameter. The RF_n values of these are between approximately 0.25 and 0.35. The surfaces of the remaining soils, also containing clods of from 50 to 100 mm diameter, are characterized by the RF_n values from approximately 0.4 to 0.5.

Soil spectral features

Representative reflectance curves for the analyzed soils in selected illumination conditions are shown in Fig. 8. The natural roughness state is compared with curves determined for the same soils but for smoothed surfaces. These curves have very different reflectance levels. The reflectance level of bright soils having low organic matter content, such as initial denudative and the typic brown podsolic soils, is approximately twice as large as for dark soils having a high organic matter content, i.e., black earths. The shape of the curves of the black earths is concave. The curve shape for the remaining test soils is convex, with a characteristic change of curvature in the range of 750–850 nm. The curves of the studied soils, regardless of whether they were for smoothed surfaces or natural rough surfaces under various illumination conditions, have an identical shape. The dif-

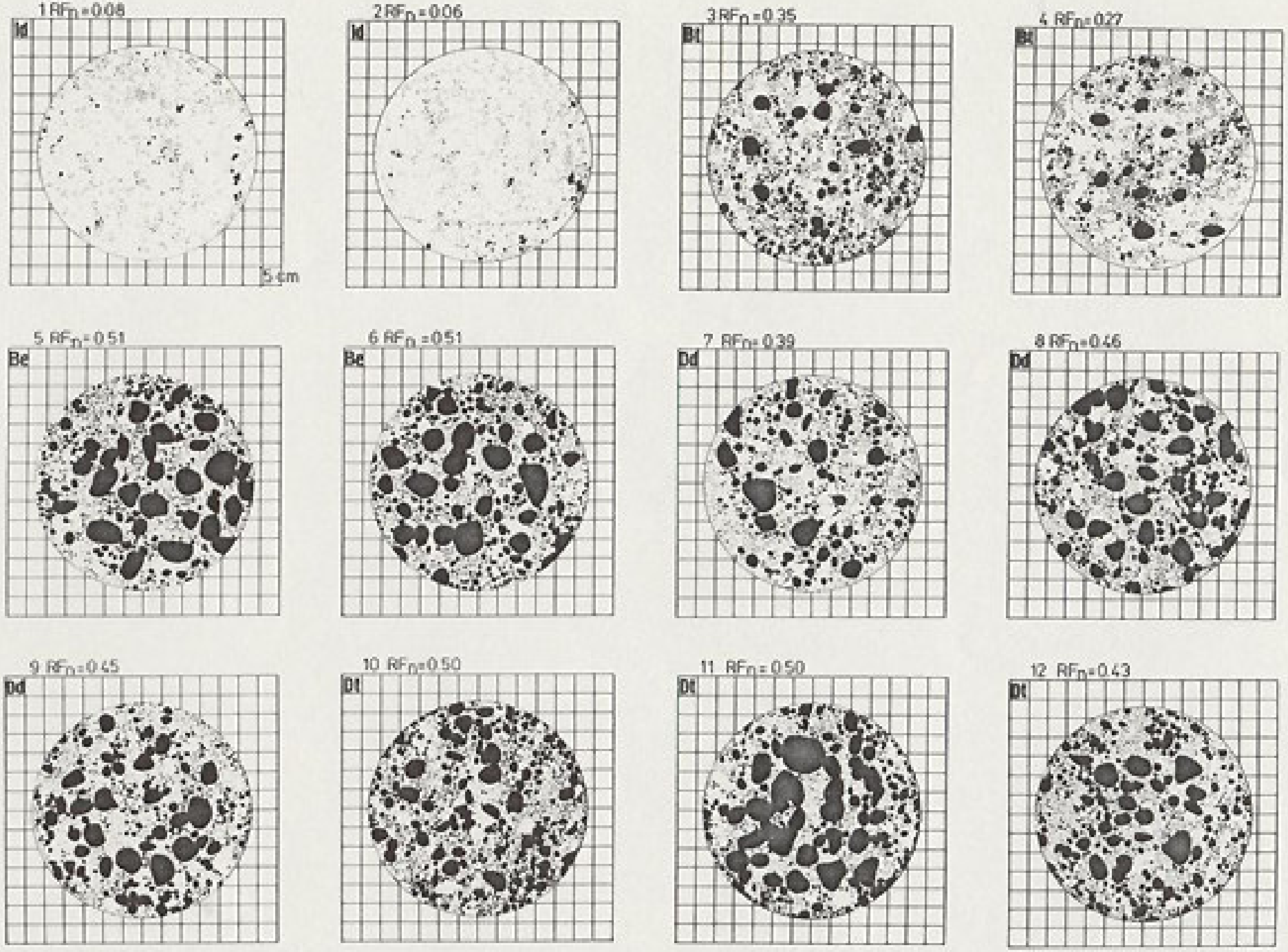

FIGURE 7. Aggregates and clods of tested rough soil samples in the spectrophotometer field of view. Symbols and numbers as in Table 3.

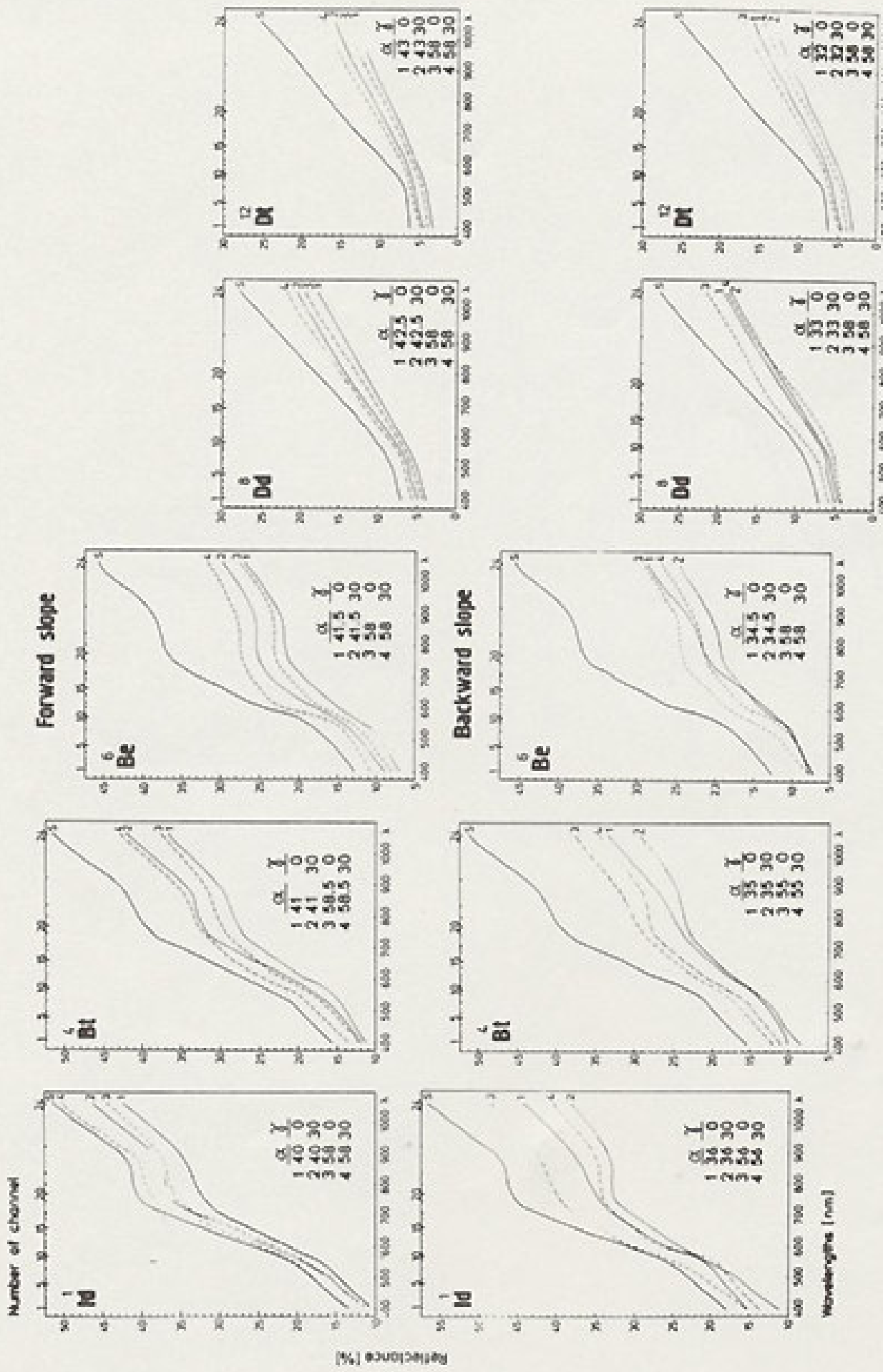

FIGURE 8. Representative reflectance curves of distinguished soils for a selected solar altitude (α), angle of plane slope (γ), and sloping of the slope towards the sunbeam direction, compared with smooth surface sample curves (S). Remaining symbols and numbers as in Table 3.

ference between them only concerns the reflectance level and is higher for light soils than for dark ones. This is particularly visible for eroded brown podsolic soils samples of high spectral brightness. All the measured samples in their natural roughness state, for both the forward and backward slopes, show reflectance dropping with the decrease of solar altitude. For forward slope, the reflectance increases with increasing slope angle, but for the backward slope it declines as this angle increases.

The accuracy of the model

The accuracy of the shadow model was tested by a linear regression analysis of the hemispherical-directional reflectance coefficients measured (R_r) and predicted by the model (R_m) of the 12 rough soil surfaces. This analysis was performed at five wavelengths of 440, 540, 640, 740, and 860 nm, using 368 spectra representing these soil surfaces under different illumination conditions (as specified in Table 2). The analysis yielded an average (for these wavelengths) correlation coefficient (r) value near 0.99 (Fig. 9). The limit of 95% confidence interval indicates that the R_m for average tested wavelengths, i.e., for 644 nm, may be calculated with the mean deviation of about $\pm 3\%$ from the R_r.

The measured rough soil reflectance coefficients related to the same soil reflectance coefficients, but smooth

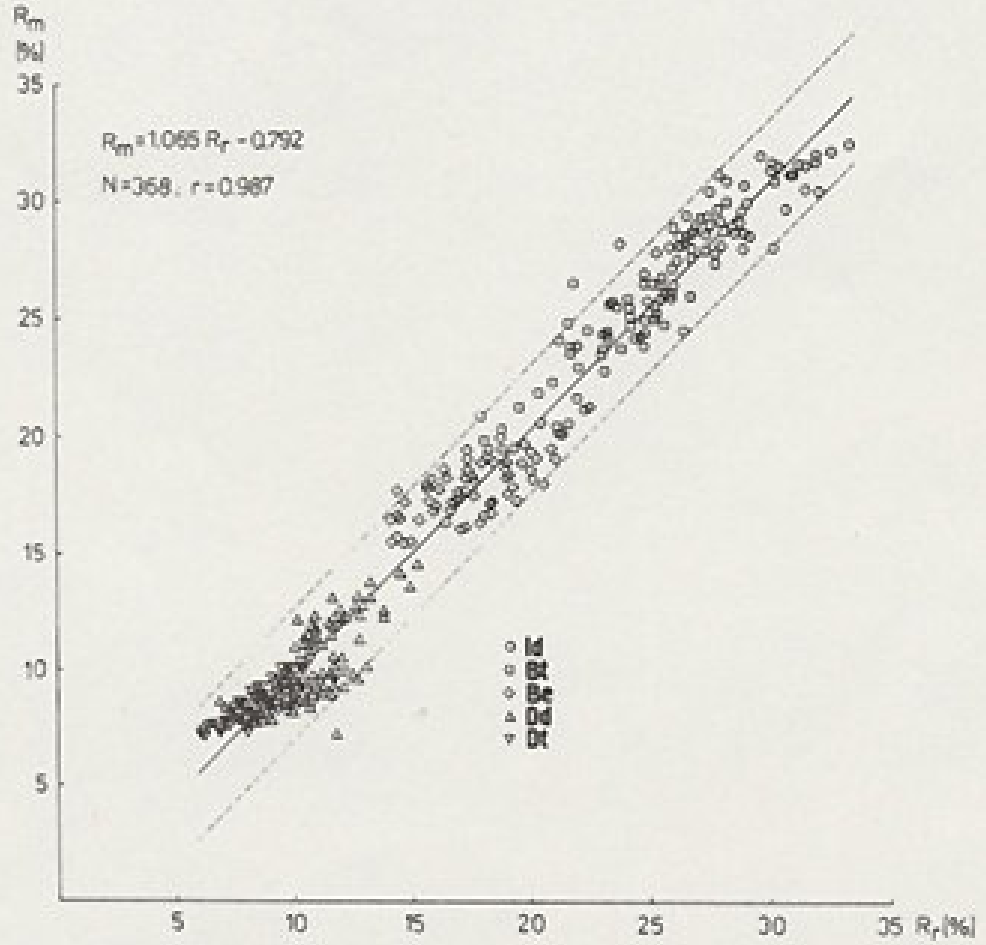

FIGURE 9. Relationship between rough soil hemispherical–directional reflectance coefficient predicted by the model (R_m) and measured by the field spectrophotometer (R_r); N = number of data points; (----) limit of 95% confidence interval; remaining symbols as in Table 3.

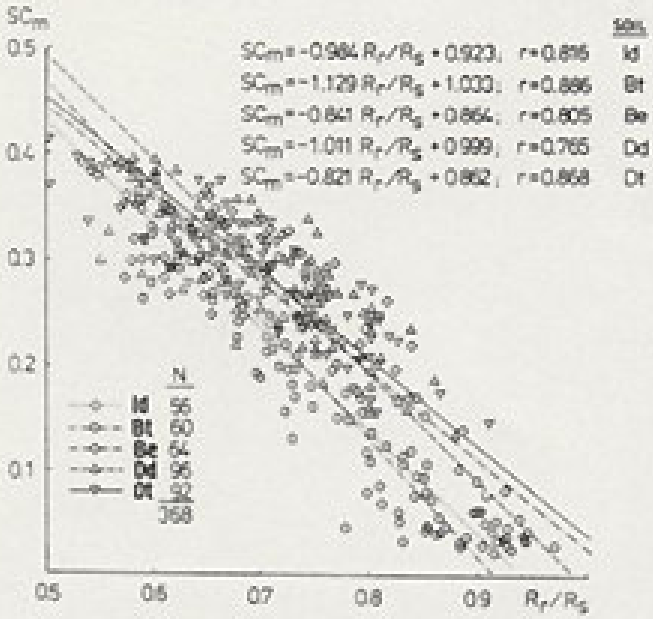

FIGURE 10. Relationship between measured rough soil reflectance coefficient related to the same but smooth soil reflectance coefficient (R_r/R_s) and predicted the soil surface shadowing coefficient (SC_m); N = number of data points; remaining symbols as in Table 3.

(R_r/R_s) analyzed vs. the predicted shadowing coefficients of these soil surfaces (SC_m) demonstrates the similarity of the relation between measured and predicted spectral data among all the five tested soils (Fig. 10). The average (for the five wavelengths) differentiation of the slope and intercept are negligible for these five soils.

Discussion

A reflectance of disturbed soil samples under laboratory conditions increases with a decrease of soil particle size. Bowers and Hanks (1965) tested the reflectance of soil materials ranging from coarse clay to sand found the character of this relationship to be exponential. Piech and Walker (1974) confirmed greater reflectance with decreasing particle size for the case of seventh sieve sizings of clay ranging from 2 to less than 0.062 mm for a range of 0.5–0.9 μm spectre.

The influence of the particle size on the spectral reflectance of undisturbed soils measured in the field is clearly lower than the influence of roughness due to soil aggregates and clods. Generally, heavy soils have a higher matter content and a great roughness, both of which produce of low reflectance. Al-Abbas et al. (1972), in discussing the use of scanner data to estimate clay content in soils, have shown a negative linear relation between clay content and soil reflectance. The aggregation and lightness of soils decreases as sand content increases. Gerbermann and Weher (1974), in investigating reflectance of different mixtures of clay and sand, found a positive linear relation between reflectance and sand content.

Studies of disturbed soil under laboratory conditions prove that the decrease of soil aggregate and clod size results in an increase of soil spectral reflectance. Orlov (from Mikhaylova and Orlov, 1986) has explained that the smaller aggregates and clods have a more spherical shape, but the larger ones have an irregular shape with a large number of interaggregate spaces and cracks where the incident light is trapped. He has shown that aggregates having a diameter greater than about 2 mm exhibit constant reflectance. This size is the minimum for aggregates, which are taken into the discussed model.

Soil roughness is one of the most unstable soil proporties. It is highest after tillage treatments and progressively decreases with rainfall. The soils with nonsaturated cation exchange capacity by calcium are susceptible to very intensive slaking phenomena (Bialousz, 1978). Van der Heide and Koolen (1980) found that the degree of soil slaking has an influence on the soil spectral level, but

not much effect on the spectral curve shape. Obukhov and Orlov (1964) have maintained that structureless soils reflect from 15 to 20% more light than soils having a well-developed structure. Sequential wetting and drying of aggregates may create a crust around them, reducing the soil roughness level. Cipra et al. (1971) have analyzed field spectroradiometrical characteristics of an Alfisol, which showed clearly higher reflectance for crusted soil than for soil with broken crust. Kondratyev and Fedchenko (1980) found that this crust developed on soil clods of diameter from 5 to 15 cm, resulting in an increase of soil reflectance of about 10–15%. They have explained that this soil brightness increase may be due to the weathering process which creates the crusted surfaces. This process progressively washes away the clay and humus, thereby revealing a greater number of light quartz particles.

The model of Cruse et al. (1980), worked out to predict a tillage effects on soil temperature, assumes that incoming direct beam energy striking the whole soil rough surface undergoes the diffuse reflection. The scattered energy which fell below the peak of adjacent soil element is reflected the second time, dropping the amount of the whole reflected radiation from the soil. It depends only on the soil roughness described by a soil random roughness parameter. This reflectance decreases as the soil roughness increases. The discussed model also takes into account illumination conditions of rough soil surface which determine the degree of soil shadowing. The shadowed soil areas which are only illuminated by scattered solar radiation decrease the amount of direct solar beam energy fallen on the soil surface. According to Reyleigh's criteria, a natural clod as well as an artificial smooth soil characterizes the same kind of reflectance. The surface height variation of the both soils is many times higher than wavelength determining division between truly smooth and rough surfaces which give specular and diffuse reflection (Ulaby et al., 1982). Taking into consideration the reflectance conformity of the smoothed and natural rough soil in relation to the direct beam radiation, the soil shadowing coefficient (SC_m) may appear to be the simplest for the mathematical description parameter of natural soils in various illumination conditions. It is calculated by the soil surface roughness parameter (RF_n) which can be evaluated by using special diagrams. The other surface parameters, as the standard deviation of surface height or the surface correlation length (Ulaby et al., 1982), are more difficult in evaluation and are useless to predict the SC_m. Generally, the hemispherical–directional reflectance coefficient of rough soils predicted by this model increases while the sun is rising. Coulson and Reynolds (1971) have found that maximum hemispheric reflectance coefficient of natural rough clay and loamy soils occurs at a sun elevation of 10–20°. The incompatibility of those results may be explained by the fact that a down-looking receptor measuring the double hemispheric reflectance senses also the diffuse skylight. Its energy in upward radiant flux at the low sun elevations is greater than the incident direct beam radiation loss caused by the self-shadowing.

Idso et al. (1975), when discussing variations of albedo measurements of smooth and raked wet and dry bare loam soils, have explained that the self-shadowing of the rough soils effects these differences.

TABLE 4 Two-Side Confidence Interval of the Modelled (ΔR_m) and the Measured Smooth (ΔR_s) Soil Spectral Data for Mean Values of the Measured Rough Spectral Data ($\bar{R}_r$) (the Data Concerns All the Studied Soil Population)

Parameter %	Wavelengths (nm)				
	440	540	640	740	860
$\bar{R}_r$	8.8	11.1	16.4	20.9	24.1
ΔR_m	3.2	4.7	5.5	8.2	8.4
ΔR_s	7.5	10.0	13.6	16.8	16.8

On the basis of field studies, Cierniewski (1984) found an exponential equation determining the contribution of shadowed soil fragments for soils having a specified clod parameter at the given solar altitude. Results of these studies have proved an importance of sun–soil surface–sensor geometries in soil spectral measurements. This has also been emphasized by Guyot (1984) and Epiphanio and Vitorello (1984). This model therefore includes the slope and aspect of the soil surface relative to the direction of solar illumination and the viewing direction. The limiting of the sensor view direction only to nadir corresponds to the center of vertical aerial photographs and other imagery.

The proposed model utilizes spectral data from smooth samples to calculate the reflectance of natural rough soil surfaces under given illumination conditions. Thus it determines simultaneously the quantitative relation between the spectral data obtained under laboratory and field condition, respectively. It should allow researchers to better understand the relationship between the spectral and physical properties of bare soils under different illumination conditions, as well as soil background influence on spectral response from crops. The correctness of this model, tested by field spectrophotometric measurements, demonstrates the ability to extend laboratory measured soil spectra data to field conditions. Stoner et al. (1980) emphasize that this ability should have important implications in applying remote sensing to soil surveys.

Conclusions

The presented model for all tested illumination conditions, including the situation when the backward slope relative to the solar altitude is lower than the angle of a given slope, demonstrates that the shadowing coefficient of soil surface (SC_m) decreases with the decrease of soil roughness. SC_m also decreases when the solar altitude increases in full interval of the altitude from 0° to 90° when the soil is on forward slopes more sloping than 20°. The model indicates that this relationship for soil slopes having a surface roughness lower than 0.5 for a specified range of solar altitude may be the opposite.

This model reduces the spectral level of rough soils under full shadowing conditions to be 1/3–1/4, the value of the maximum for soils, but the shape of soil spectral curves does not significantly change.

Linear regression analysis, used to determine the average accuracy of this model for five chosen wavelengths, indicates that the correlation coefficient of the relationship between all 368 data points measured and calculated using this model reaches a value of approximately

0.99. It has been found that the relation between measured and predicted reflectance coefficient is similar for all the five tested soils.

This work was supported by the Institute of Land-Surveying and Cartography in Warsaw.

References

Al-Abbas, A. H., Swain, P. H., and Baumgardner, M. F. (1972), Relating organic matter and clay content to the multispectral radiance of soils, *Soil Sci.* 114:477–485.

Belonogova, I. N., and Tolchelnikov, Y. S. (1959), On the dependence of the brightness of minerals on the degree of dispersion, *Izv. Akad. Nauk SSSR, Ser. Geol.* 11:98–101 (in Russian).

Bialousz, S. (1978), Application of photointerpretation to mapping of soil drainage conditions, *Prace Komisji Naukowych PTG* V/35:1–143 (in Polish).

Bowers, S. A., and Hanks, R. J. (1965), Reflection of radiant energy from soils, *Soil Sci.* 100:130–138.

Cierniewski, J. (1984), Influence of surface soil clod structure on spectral response of soil cover, *Colloques l'INRA* 23:141–148.

Cierniewski, J. (1986), Mathematical model of soil spectral reflectance in the visible and near-infrared range including destruction of surface soil cloddiness under rainfall, *ITC J.*, forthcoming.

Cipra, J. E., Baumgardner, M. F., Stoner, E. R., and MacDonald, R. B. (1971), Measuring radiance characteristics of soil with a field spectroradiometer, *Soil Sci. Soc. Am. Proc.* 35:1014–1017.

Coulson, K. L., and Reynolds, D. W. (1971), The spectral reflectance of natural surfaces, *J. Appl. Meteorol.* 10:1285–1295.

Cruse, R. M., Linden, D. R., Radke, J. K., Larsen, W. E., and Larntz, K. (1980), A model to predict tillage effects on soil temperature, *Soil Sci. Soc. Am. Proc.* 4:378–383.

Egbert, D. D., and Ulaby, F. T. (1972), Effect of angles of reflectivity, *Photogramm. Eng.* 38:556–564.

Epiphanio, J. C. N., and Vitorello, I. (1984), Inter-relationships between view angles (azimuth) and surface moisture and roughness conditions in field-measured radiometer reflectance of an oxisol, *Colloques l'INRA* 23:185–192.

Gerbermann, A. H., and Weher, D. D. (1979), Reflectance of varying mixtures of a clay soil and sand, *Photogramm. Eng. Remote Sens.* 45:1145–1151.

Guyot, G. (1984), Angular and spatial variability of spectral data in the visible and near infrared, *Colloques l'INRA* 23:27–44 (in French).

Heide van der, G., and Koolen, A. J. (1980), soil surface albedo and multispectral reflectance of short wave radiation as a function of degree of soil slaking, *Neth. J. Agric. Sci.* 28:252–258.

Idso, S. B., Jackson, R. D., Reginato, R. J., Kimball, B. A., and Nakayama, F. S. (1975), The dependence of bare soil albedo on soil water content, *J. Appl. Meteorol.* 14:109–113.

King, C. (1984), Bare soils spectral qualities: analysis of radiometric spectra acquired on the ground in Bassin parisien, *Colloques l'INRA* 23:253–264 (in French).

Kondratyev, K. Y., and Fedchenko, P. P. (1980), Recognition of soils by their reflectance spectra, *Pochvovedenije* 12:47–53 (in Russian).

Mikhaylova, N. A., and Orlov, D. S. (1985), *Optical Features of Soils and Soil Component*, Nauka, Moscow, pp. 35–38 (in Russian).

Obukhov, A. I., and Orlov, D. S. (1964), Spectral reflectivity of the major soil groups and possibility of using diffuse reflection, *Pochvovedenije* 2:83–94 (in Russian).

Piech, K. R., and Walker, J. E. (1974), Interpretation of soils, *Photogramm. Eng.* 40:87–94.

Stoner, E. R., Baumgardner, M. F., Weismiller, R. A., Biehl, L. L., and Robinson, B. F. (1980), Extension of laboratory-measured soil spectra to field conditions, *Soil Sci. Soc. Am. Proc.* 44:572–574.

Ulaby, F. T., Moore, R. K., and Fung, A. K. (1982), *Microwave Remote Sensing Active and Passive* Addison-Wesley, Reading, MA, Vol. II, pp. 822–827.

Received 24 July 1986; revised 12 May 1987